

Full-Field Deformation Measurements in Liquid-like-Solid Granular Microgel Using Digital Image Correlation

A. McGhee¹ · A. Bennett¹ · P. Ifju¹ · G.W. Sawyer^{1,2} · T.E. Angelini^{1,3}

Received: 15 March 2017 / Accepted: 23 August 2017 / Published online: 7 September 2017
© Society for Experimental Mechanics 2017

Abstract This paper presents the experimental characterization of the in-plane deformation field at any depth within a granular support medium (GSM) called Carbomer 940 using digital image correlation (DIC) and particle image velocimetry (PIV). A method was developed to produce a 2D plane of randomly shaped speckles within the GSM for DIC. Four different needle diameters and four different speeds were used as test specimens representative of those utilized for 3D printing of soft matter in the GSM. The results can be used to determine dimensional tolerances and assessing interactions between multiple injection needles and acceptable spacing. The displacements in the direction of needle motion (u) and transverse (v) were obtained. Subsequently, the magnitudes were determined as a function of distance from the needle path and time history. Results show that near the needle there is a region of yielded/fluidized material and away from the needle path the material acts like a viscoelastic solid. Permanent deformation decreases with increased distance from the path and recovery is enhanced by reversing back through the path.

Keywords 3D printing · Digital image correlation · Herschel-Bulkley · Soft matter · Yield stress

✉ A. McGhee
mcghealex@ufl.edu

¹ Department of Mechanical and Aerospace Engineering, University of Florida, Gainesville, FL 32611, USA

² Department of Materials Science and Engineering, University of Florida, Gainesville, FL 32611, USA

³ J. Crayton Pruitt Family Department of Biomedical Engineering, University of Florida, Gainesville, FL 32611, USA

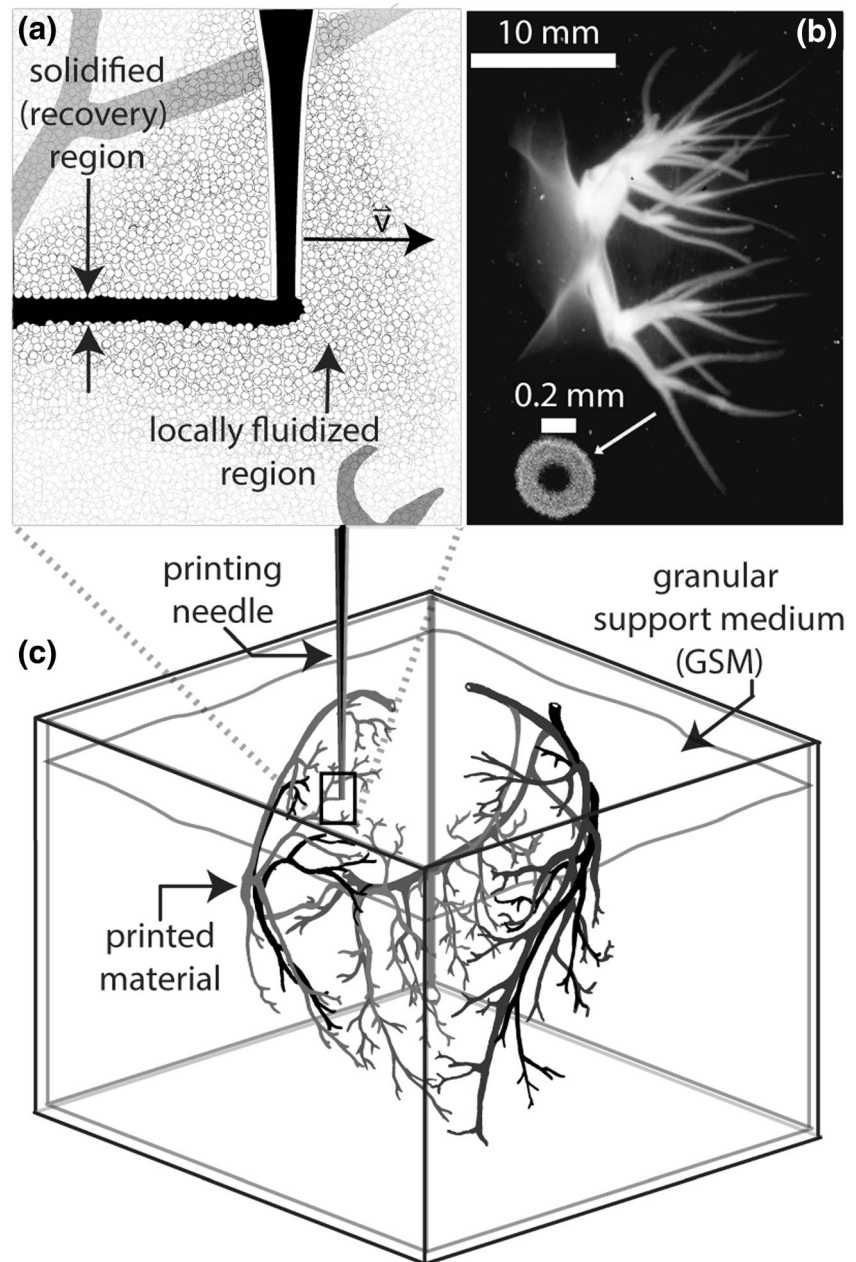
Nomenclature

DIC	Digital image correlation
PIV	Particle image velocimetry
GSM	Granular support medium
n	Flow index
k	Consistency index
τ_0	Yield stress
$\dot{\gamma}$	Strain rate
Re	Reynolds number
Od	Oldroyd number
ρ	Density
V	Velocity
D	Diameter
(w/w)	Ratio of weight to weight

Introduction

The ability to print soft matter is confounded by the print materials ability to support itself in a open environment. Recently a technique has been developed at the University of Florida that allows for soft materials to be 3D printed [1]. By using an extrusion needle and a granular micro-hydrogel medium as a support material, soft matter structures of incredible complexity can be 3D printed as shown in Fig. 1. Currently, slow raster speeds and small needle diameters are required to obtain high part accuracy, and this constraint restricts the speed of the printing process. Once printing begins, precision becomes a race against time since printed material can migrate from its desired position after the long time periods needed to print complex objects. A multiple needle approach is being developed to overcome this constraint, but the increase in printing needles may come at a cost. Each needle deforms the volume of granular support medium with elastic and plasticly deformed regions. If a

Fig. 1 An example of the structures that can be printed within the microgel medium. (a) As the needle is dragged through the surrounding granular medium, it yields allowing for the deposition of print material then recovers trapping the printed material in place. (b) A 3D printed structure made of a crosslinked polymer freely floating in water along with an inset confocal cross section [1] (c) An artist's rendering of the printing setup



material is extruded in a region elastically deformed by another needle, then the printed material will move as the GSM elastically recovers, thereby introducing a position error. This volumetric deformation can be taken into account during the path planning by introducing an offset to the printing needle based on the other needle's predicted deformation. The amount of offset introduced will need to be a function of needle geometry and kinematics. Alternatively, a path planning method based on the radial distance each printing needle will need to stay away from each other to impart nominal effects on one another can be employed. For either path planning method, the need to fully define the deformation caused by various needle diameters and speed combinations is apparent.

This paper introduces a digital image correlation (DIC) technique to measure in-plane deformations at a desired depth within the volume of GSM. The GSM is comprised of cross-linked poly(acrylic acid) copolymer that is extremely hydrophilic and swells when added to water creating a gel made of many individually swollen particles with a cross section of approximately $10\ \mu\text{m}$. This gel forms a jammed solid with material properties that are dependent on the polymer concentration and pH [2]. Rheological studies of this material show a Herschel-Bulkley model provides the best fit for the yield stress versus shear rate [3]. The properties of this gel enable a unique solution to the problem of 3D printing soft materials. As the needle moves through the volume, the GSM particles rearrange allowing deposition of print material. As the needle moves away, the GSM

particles conform around the print material locking it in place (Fig. 1). The process of 3D printing into the granular medium is described thoroughly in the literature [1, 4–9].

There has been a large body of work attempting to characterize the flow of a yield stress material around spherical and cylindrical objects in an infinite plane by using particle image velocimetry (PIV) and numerical simulations [10–20]. The PIV technique used in these studies employs glass beads (which have uniform shapes) suspended in the GSM and a laser sheet which illuminates only the glass beads in a plane within the medium. As objects of interest move through the GSM, the beads are displaced, and a sequence of images are taken to capture the deformation in time. To realize the limitations of this method, imagine tracking the location of similar looking objects as they move around a table. Two parameters which affect the ability to track these objects are their density, and the frequency at which the objects are imaged. As an extreme case, if all of the objects moved such that the locations of each object shifted exactly to their neighbor's location from one frame to another the images would look the same, and the conclusion would be that there was no motion. Although this method has some limitations, it can be used if the mean particle displacement per frame is within an optimal threshold largely dependent on the particle density, and thus the desired spatial resolution of the resulting velocity field [21]. There is a limit to the resolution with this method, however, since increasing the glass bead density will introduce unintended effects to the deformation. Tracking large deformation with a speckle pattern consisting of uniformly shaped speckles is possible, but would require data to be collected and analyzed above the Nyquist sampling rate needed for lossless digitation of particle movement, and would be hindered by an accumulation of measurement error [22, 23].

Here we introduce a method which allows a speckle pattern with randomly shaped speckles to be used for in plane displacement measurements within a yield stress material. We have limited this manuscript to measure 2D in-plane deformation since this is the most basic DIC analysis method, and serves as a foundation for all future improvements. The material used to create the speckle pattern is more closely matched to the modulus of the material being tested, and only exists in a single plane; this allows for a high density speckle pattern, and translates to a higher resolution deformation measurement than previous methods. The introduction of randomly shaped speckles allow for direct displacement measurements at a broad range of displacement and time scales.

Experimental Method

Here, we develop a method which allows for measurement of the global in-plane deformation due to a needle moving in a straight line within a volume of the GSM. Traditionally DIC

utilizes a speckle pattern attached to the surface of a material, however in this case, we are interested in capturing the in-plane displacement field at a depth within a medium; to do this, a speckle pattern plane is printed at the desired depth using a 3D printer. The speckles are made of a polymer cured with black paint and blended with the Carbomer. The polymeric speckle-Carbomer mixture is placed into a syringe which is loaded into a 3D printer designed to extrude the contents of the syringe at a specified x, y, z position (Fig. 2). Just above the speckle pattern, we print a layer of white paint pre-mixed with the GSM; this layer serves as a background for the speckle pattern. The methods used in this paper can be applied to all types of yield stress materials so long as the speckle pattern can be imaged within the media.

The container which holds the GSM is a $60 \times 60 \times 40$ mm plastic container which is sufficiently large enough for wall effects to be negligible in our measurement [24]. The container that we used was carefully selected to have a very flat bottom surface. Since the wall does not feel the effects from the needle as it moves through the middle of the volume, we can assume that the needle is deforming an infinite plane of the GSM.

Creation of the GSM

Carbomer 940, distributed by MakingCosmetics Inc. was mixed with ultra-pure water at a concentration of 0.1% (w/w). The

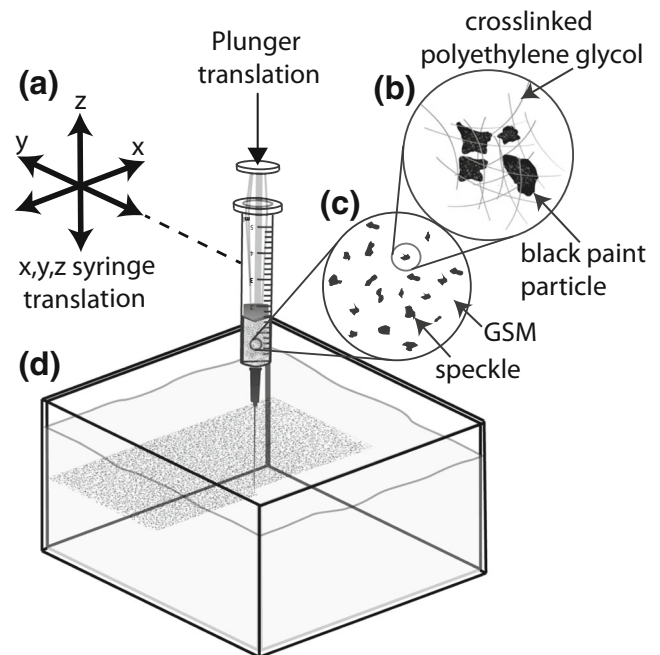


Fig. 2 (a) the 3D printer is represented by a set of vectors which control the x, y, z translation of the entire syringe, as well as the displacement of the plunger. (b) Each speckle consists of black paint particles that are crosslinked into PEG (c) inside the syringe, the black crosslinked speckles are mixed with the GSM. (d) The syringe moves in a raster pattern while the plunger is displaced to force the GSM-speckle mixture into the volume of GSM at the desired plane

Carbomer water dispersion was centrifugally mixed for ten minutes at 3500 rpm and 22 °C until the Carbomer was completely suspended. Sodium hydroxide was added to the suspension to raise the pH to 6.20. The suspension was then mixed with a paddle mixer for 5 min and allowed to rest for 24 h to ensure homogeneity. The solution was then centrifugally mixed for 15 s at 3500 rpm to remove trapped air bubbles caused by paddle mixing. Since the yield stress is a strong function of both concentration and pH [2], each batch of Carbomer has slightly different characteristics. Thus, the Carbomer was tested in a Kinexus KINX2100 rheometer to measure the shear rate versus the yield stress, as well as the thixotropic time.

Creation of White Background Material

The GSM was mixed with Spectra Tex 56–146 Opaque Intense White water-based paint at a 5:1 ratio to make 10 mL. To ensure that the paint did not diffuse out of the microgel suspension, a layer of the GSM was placed into a petri dish along with the paint-microgel suspension. The specimen was monitored for one week, and we found that the boundary between the two layers remained unchanged. After four weeks, we found that there was only a slight amount of paint migration. For the relatively short time periods needed to run these DIC experiments, any migration of the white paint layer was therefore deemed negligible.

Creation of the Black Polymeric Speckles

To create a speckle pattern in the middle of the volume of the GSM, small black particles need to be extruded through a needle tip at the desired location. Hard particles tend to form agglomerations in the shape of an arc within the needle which causes a jam. Additionally, many hard particles such as graphite are hydrophobic and tend to clump together. To overcome this problem, a flat hydrophilic and flexible particle was created using polyethylene glycol (PEG) mixed with black paint and Irgacure (Fig. 2(b)). The PEG-paint particles were created using the following procedure. Using polyethylene (glycol) diacrylate (PEG-DA) average Mn 700 g/mol and polyethylene (glycol) acrylate (PEG-A) average Mn 480 g/mol, stock solutions are made with concentrations of 400 mg/mL PEG-DA in ultrapure water, and 615 mg/mL of PEG-A in ultrapure water. The resulting stock solutions are mixed using concentrations of 20% (w/w) PEG-DA and 80% (w/w) PEG-A to form the resulting polymer solution. Next, a stock solution of Irgacure (2-Hydroxy-4'-(2-hydroxyethoxy)-2-methylpropiophenone) is made with a concentration of 0.125 g Irgacure to 1 ml of ethanol. The final solution uses 24.5% (w/w) polymer solution with 74% (w/w) ultrapure water along with 0.5% (w/w) Irgacure solution and 1% (w/w) Spectra 56–146 Opaque Jet Black water based paint. The resulting solution should be vortexed for 1 min then thinly spread onto a glass sheet and

photo-initiated for 3 min under a 400 W, 420 nm wavelength UV curing lamp and set aside for 2 h to fully cure. The resulting film is then placed into a blender along with water to create particles which range in size from 200 to 300 μm . After dehydrating the water-particle mixture, the particles are then added to the GSM to create a suspension.

Setup of the Specimen

Using a four axis 3D printer capable of holding a syringe and displacing the plunger in a controlled manner, the contents of the syringe can be accurately extruded within the GSM as shown in Fig. 2(a). The syringe was loaded with the microgel-PEG suspension and printed in a raster pattern in a 50 \times 50 mm square in the middle of the volume (Fig. 2(c) and (d)). The flowrate of the microgel-PEG suspension was 2500 $\mu\text{L}/\text{min}$ with a translation speed of 30 mm/s which, through volume conservation and the assumption that the print material is cylindrical gives a plane thickness of 0.17 mm. The thickness of the speckle plane can be lessened by increasing the density of the PEG speckles in the printing needle which allows for a decrease in flowrate to keep a similar in-plane speckle density. A plane of white background material is then printed using a raster pattern measuring 60 \times 60 mm with a distance of 5 mm above the speckle pattern. To ensure no out-of-plane distortion of the speckle pattern occurs, the printing needle is inserted and retracted near the boundary of the container. An exploded assembly of the specimen which shows the speckle and white paint layers is illustrated in Fig. 3.

To control the translation of a needle through the speckle pattern as seen in Fig. 4, a PI M-605.2DD servo motor was used along with a Mercury C863 DC motor controller. This servo-controller combination allows for a positioning accuracy of 0.1 μm with a maximum velocity of 50 mm/s and a minimum incremental motion of 0.3 μm . Attached to the servo motor stage is an L bracket that holds a syringe. The needles used in this experiment are stainless steel dispensing needles with a luer lock connection from McMaster-Carr and attach to a syringe which is mounted to the L bracket. This setup is placed on top of a translucent acrylic plastic which is bolted to the surface of a table. Directly under the line of motion of the needle, an Image Source DMK23GM021 1.2 M-pixel camera with a Nikon 50 mm 1:1.4G lens is pointed vertically upwards. The specimen containing the speckle pattern is then placed above the camera, and the camera is focused on the speckle pattern. Using this experimental setup, shown in Fig. 5, images were captured at the rate of 0.1, 1, 10, and 100 frames per second as the needle was translated at speeds of 0.01, 0.1, 1, and 10 mm/s respectively for 50 mm through the speckle pattern then returned to the initial position. This image capturing scheme allows for similar spatial distance traveled per frame. The camera orientation with respect to the region we were testing was always within 3 degrees to normal.

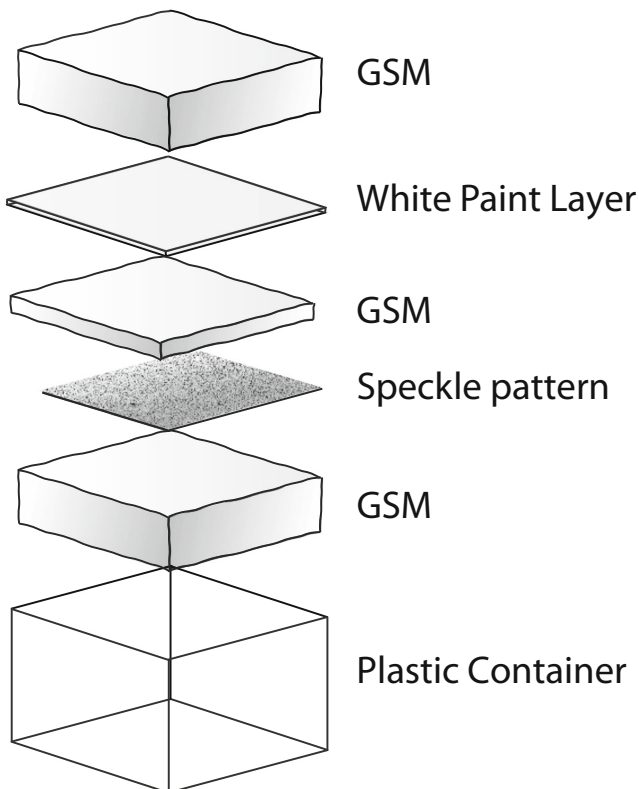


Fig. 3 An exploded view of the layers within the volume of interest. The speckle pattern is printed into the granular medium; then a white paint layer is printed leaving space between the printed layers

It is important to note that the test specimen was reused for multiple experiments. Although Carbomer 940 has been shown to have memory of the shear history of previous experiments [25], the effect of the previous experiment runs contributed insignificant but measurable effects on the displacement results; this effect can be seen in Fig. 7 as a small bulge in the displacement field ahead of the needle path. This bulge is not seen in the experiments that used a fresh sample, and are seen in the experiments that had previous runs along the same path.

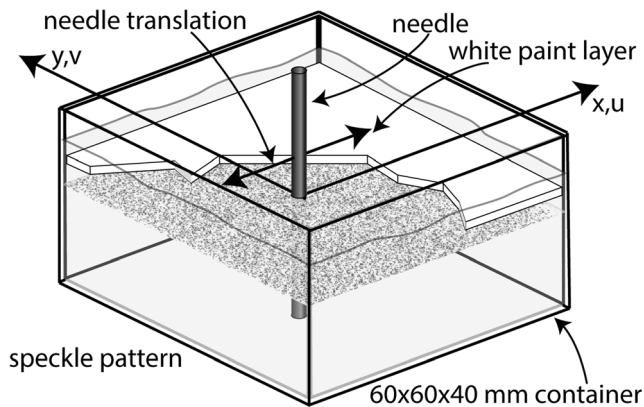


Fig. 4 The test specimen and needle translation path is shown without the white paint payer so the speckle pattern-needle interaction can be seen

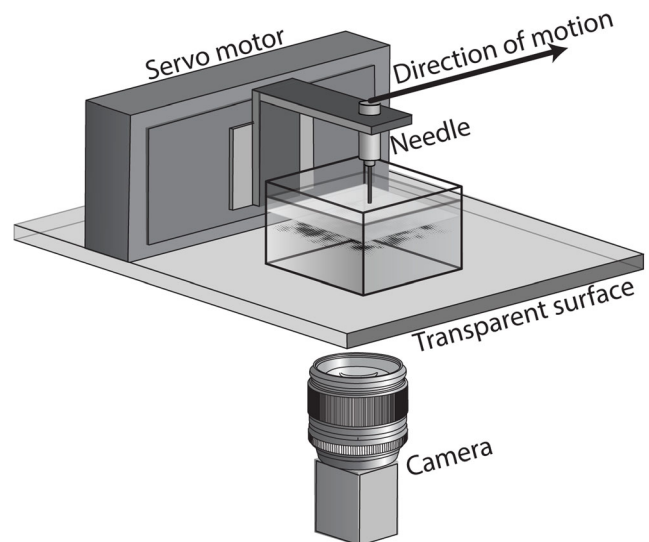


Fig. 5 The setup of the experiment showing the placement of the camera, and servo motor with respect to the specimen

Results

The Carbomer was tested in a Kinexus rheometer to measure the shear rate versus the yield stress, as well as the thixotropic time. The thixotropic time, a measure of the time needed for the material to go from a yielded state to an unyielded state as a constant stress, lower than the yield stress, is applied, was measured to be 3 s. Using a rough plate and cone to measure the shear rate and shear stress and then fitting the Herschel-Bulkley model equation (1) to the resulting data points, the following material properties were found $n = 0.43 \pm 0.03$, $k = 3.2 \pm 0.6 (Pa \cdot s^n)$, $\tau_o = 13.3 \pm 0.7 (Pa)$. (+/- correspond to 95% confidence intervals from non-linear least squares fit.

$$\tau = \tau_o + k\dot{\gamma}^n \tag{1}$$

These parameters are then used to calculate the Reynolds number, the ratio of the inertial effects to the viscous effects, defined by equation (2) as well as the Oldroyd number equation (3) which is the ratio of the plastic effects to viscous effects.

$$Re = \frac{\rho V^{2-n} D^n}{k} \tag{2}$$

$$Od = \frac{\tau_o}{k(\frac{V}{D})^n} \tag{3}$$

The approximate Reynolds and Oldroyd numbers were calculated for each needle diameter and velocity combination and listed in Table 1.

The images to be analyzed were selected such that the needle was roughly in the middle of the volume and moving at a constant velocity. The image sequence spacing was selected such that the distance traveled by the needle would be 1 mm per image with 11 total sequential images. These images

Table 1 The approximate Reynolds number (Re – inertial: viscous) and the Oldroyd number (Od – plastic: viscous) of the GSM in response to various needle diameter and speeds

D	$V = 0.01$ mm/s		$V = 0.1$ mm/s		$V = 1$ mm/s		$V = 10$ mm/s	
	Re	Od	Re	Od	Re	Od	Re	Od
0.40 mm	1 e-7	23	6 e-06	8	2 e-04	2	7 e-03	1
0.81 mm	2 e-7	32	8 e-06	11	3 e-04	4	1 e-02	1
1.27 mm	2 e-7	39	1 e-05	14	3 e-04	4	1 e-02	1
1.82 mm	3 e-7	46	1 e-05	16	4 e-04	5	1 e-02	2

were then processed using Ncorr [26], a 2D open source DIC application for MATLAB, to obtain the deformation and strain fields. The needle translates independently of the camera, so the resulting displacement field moved with the needle throughout each image as it deforms and elastically recovers. Since the movement of the needle was at a steady state, the displacement caused by the needle in each frame was assumed to be at steady state. After tracking the location of the needle in each image, the displacement field for all measurements were aligned with each other using the center of the needle as a reference and cropped such that the field only included a 25×25 mm area around the needle. Recentering the displacement field allows us to make statistical measurements such as the standard deviation and mean of the data for each needle diameter and speed combination.

The u and v components of the displacement field as well as the magnitude of displacement for the 0.8 mm needle at 1 mm/s are presented in Fig. 6. All v -displacement values above the path are positive and all values below the path are symmetrically negative, so the absolute value of the v -displacements are displayed to increase the resolution of the far field. The magnitude of displacement plot shows how far away from the needle the GSM is affected.

A plot of the mean displacement magnitude due to an increase in needle diameter and speed, using a constant scale for all images, is shown in Fig. 7. The needle size and location is

marked by a black circle in each image. A set of 16 contour lines which form ellipsoids that are tangent to the center of the needle and increase in diameter overlay each plot. Directly behind the needle, the resulting deformation is decorrelated due to a fluid-like distortion of the speckle pattern. This decorrelated region contains erroneous data and has been excluded from all plots by setting the displacement to zero in that area. From the results presented in Fig. 7, we can conclude that the magnitude of displacement due to a needle moving through the granular medium is strongly dependent on diameter and weakly dependent on velocity.

Figure 8 shows the u -displacement versus distance away from the leading edge of the needle. In the area directly ahead and in the path of the needle there is no v -displacement, so the u -displacement plot is essentially a magnitude of displacement plot as well. Although there is a large disparity in the magnitude of displacement close to the needle, the far field data converges to relatively the same value. This data does not collapse into a linear relationship when plotted on a semilog or log-log scale, so the full-field curves do not follow a power law or exponential model.

Figure 9(c) and (d) shows the u and v -displacement for the 0.81 mm needle at 1 mm/s along lines parallel to the path of the needle and equally spaced out by distances equal to the diameter of the needle in the direction perpendicular to the needle path (Fig. 9(a)). From the u and v -displacements, the magnitude of displacement was calculated and plotted in the same fashion. The displacements along the needle path through the third diameter away are much larger than the displacements shown which are 4–14 diameters away. To magnify the far field behavior, the first three diameter distances were not plotted. From these plots, we can see that the far field displacement falls off to approximately $50 \mu\text{m}$ after fourteen diameters (for reference a fully swollen Carbomer cell is roughly $10 \mu\text{m}$). After duplicating these same plots for all needle diameter and speed combinations, the shape of the curves were found to be similar but the magnitude scaled.

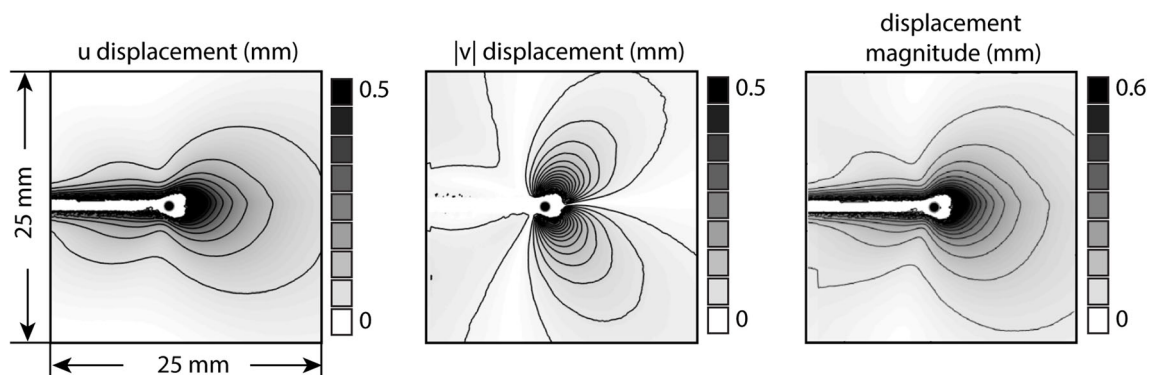


Fig. 6 The u , v , and magnitude of displacement for the 0.81 mm needle at 1 mm/s. The absolute value of the v -displacement has been displayed in order to gain more resolution in the displacement field

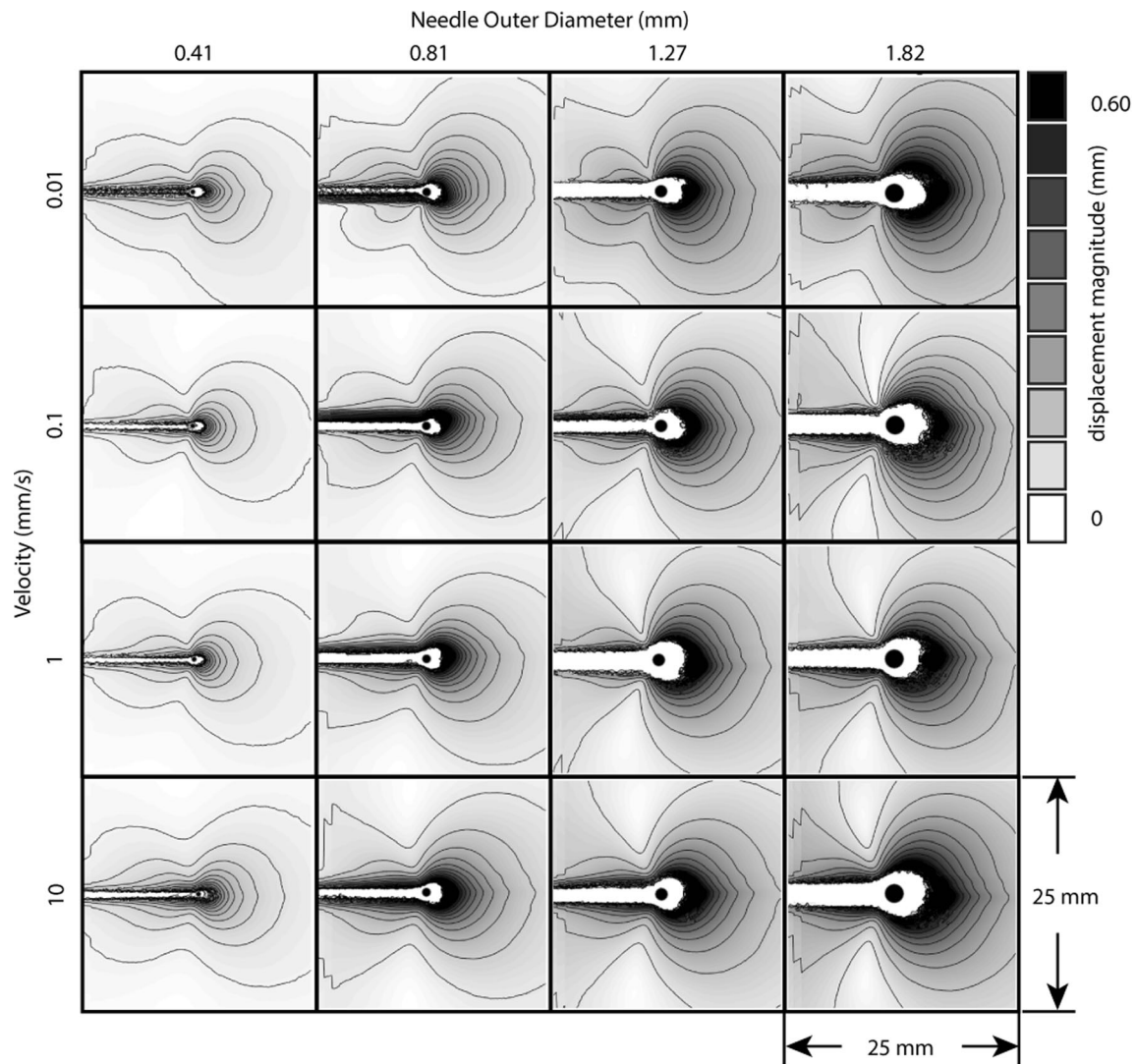


Fig. 7 The average of 11 magnitude of displacement fields of each needle diameter and needle speed combination using a constant scale

From the magnitude of displacement along parallel paths (Fig. 9(b)), the maximums were found and plotted against the radial distance from the center of the needle to the point where the maximum is located (Fig. 10). From this figure, we can see that the far-field displacement converges to a displacement of $30\ \mu\text{m}$ at $17\ \text{mm}$, or approximately 20 diameters away from the needle center. Also note that the displacement magnitude approaching the needle approximately equals the needle diameter.

Figure 11 shows the time history of the magnitude of displacement for particles at the midpoint of the needle path in the x-direction and 2–20 diameters perpendicular to the needle path in the y-direction. The needle moves through the entire volume from 0 to 60 s and then returns to the initial position from 60 to 120 s. The results show that the deformations return to almost zero as the needle retraces its path. Interestingly, the difference in peak to

peak displacement is approximately equal to the deformation at the point of reversal.

A highly magnified image of the speckle pattern as the needle passes through can be seen in Fig. 12. In this figure, elements are drawn as four-sided polygons with each corner defined by the corner of a speckle. The needle is shown as a black circle and deforms each element as it passes through the medium.

The deformation of each element as the needle moves through can be seen in Fig. 13. By numbering each element and tracking their deformation over 7 frames, we can define regions of elastic and fluid regimes. Element 1 begins behind the needle and undergoes a contraction in volume as the needle moves away. Element 2 and 3 are in the path of the needle, and both undergo 90° rotation as well a large amount of strain for the two speckles that contact the needle. Elements 4 and 5 undergo a slight shape change as well as a change in location

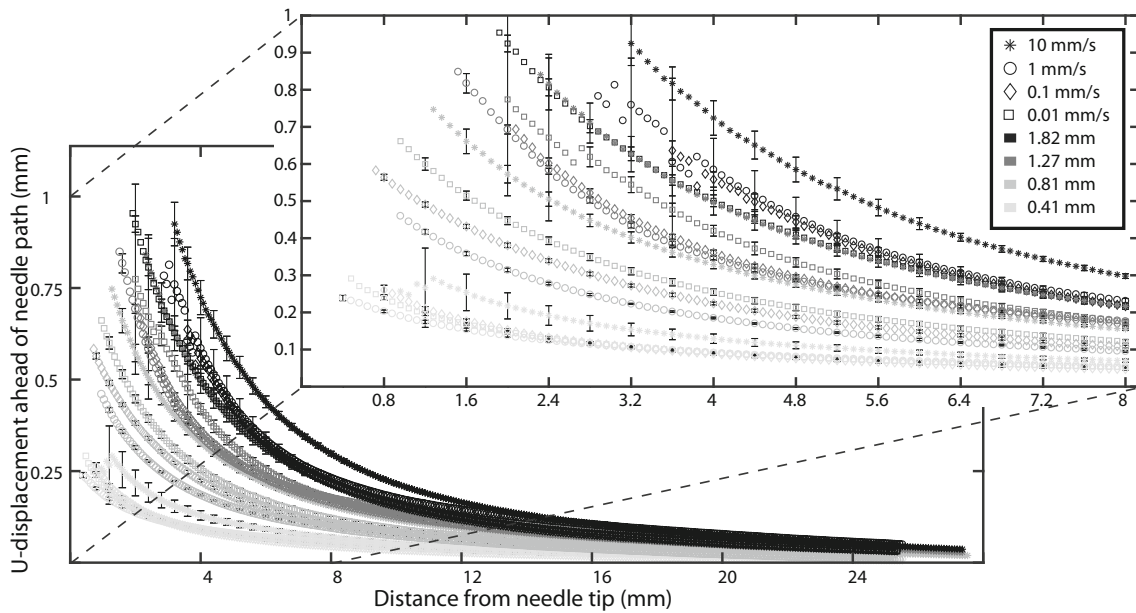


Fig. 8 The u-displacement directly ahead of the needle tip. Information from the decorrelated region was excluded

first moving further from the path of the needle, then settling closer to the path of the needle as it moves away. It is important to note that elements 2 and 3 undergo a fluid-like deformation whereas elements 1, 4, and 5 undergo solid-like deformations.

As the needle moves through the speckle pattern, some of the speckles near the needle experience fluid-like deformation. The software used to correlate the deformation cannot handle this type of deformation, so the

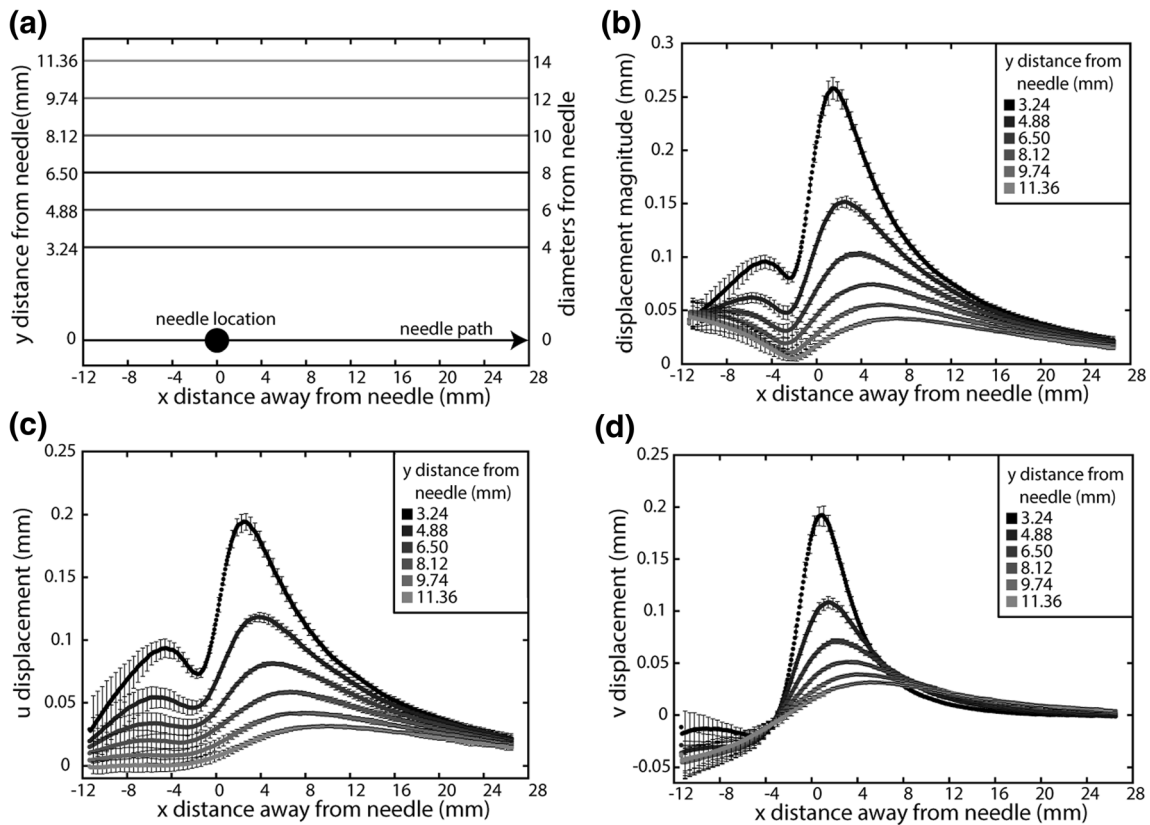


Fig. 9 The displacements plotted along lines parallel to the path of the needle and various distances away from the needle for (a) the locations of the parallel lines, (b) the magnitude of displacement (c) the u-displacement, and (d) the v-displacement

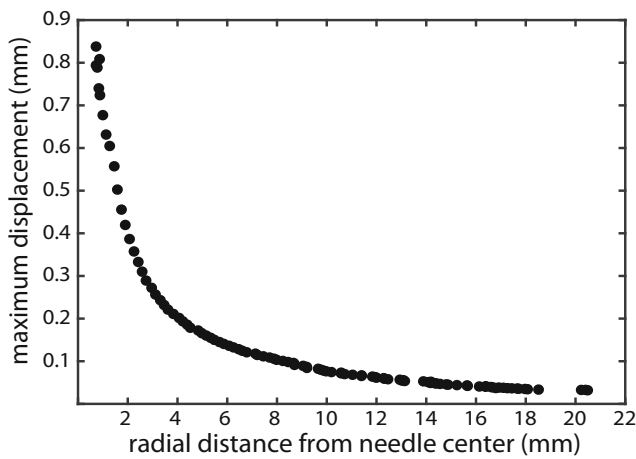


Fig. 10 The maximum values of the magnitude of displacement at radial distances away from the needle

information in this region becomes decorrelated. The width of this decorrelation region was measured and normalized by the corresponding needle diameter for each velocity and diameter combination Fig. 14. The result of this analysis shows that the width of the decorrelation normalized by the needle diameter increases slightly with increasing velocity, but decreases with increasing diameter.

Although the primary motivation for performing this study is to document displacement fields, The deformation results can be used to measure the strain fields. The strain fields for the 0.81 mm diameter needle at 1 mm/s are presented in Fig. 15. The strain in the x and y directions, as well as the shear strain, are displayed using a constant scale. The maximum shearing strain (γ_{max}) is also presented, which incorporates all of the strain types and highlights areas of highest strain.

The speckle pattern used for the DIC analysis can also be utilized to perform PIV analysis and was done using a MATLAB application called PIVlab [27]. The results of the PIV analysis can be seen as a strain and shear rate field with superposed velocity vectors in Fig. 16. The velocity vectors show there is a vortex at 45 degrees on either side of the needle which is due to the GSM being pushed out of the way, and then entering the collapsing region behind the needle. Directly in front of the needle, the velocity matches the needle speed and dies off quickly.

Discussion

The results show that this technique can produce high-quality results in both DIC and PIV analysis and is capable of measuring displacements on the order of 10 μm with a noise floor of approximately 2 μm . This technique can easily produce higher quality results by increasing the resolution of the imaging camera and modifying the setup to measure out-of-plane distortions. From Fig. 7, we can see that for the first two needle diameters, 0.40 and 0.81 mm, the contour lines form almost perfect circles, whereas the last two diameters, 1.27 and 1.82 mm, have elliptical shapes. The cause of this elliptical shape is unknown but may be a result of the container being too small for the needle – in which case the infinite plane assumption begins to fail. Surprisingly, even the smallest diameter needle had 20 μm displacement near the boundary at 50 diameters away. Future experiments will be conducted with larger containers in the attempt to find the zero displacement radius.

Previous work related to the analysis of falling spherical particles and flows around a cylinder in yield-stress materials show similar PIV results [13, 17] to our analysis seen in Fig. 16.

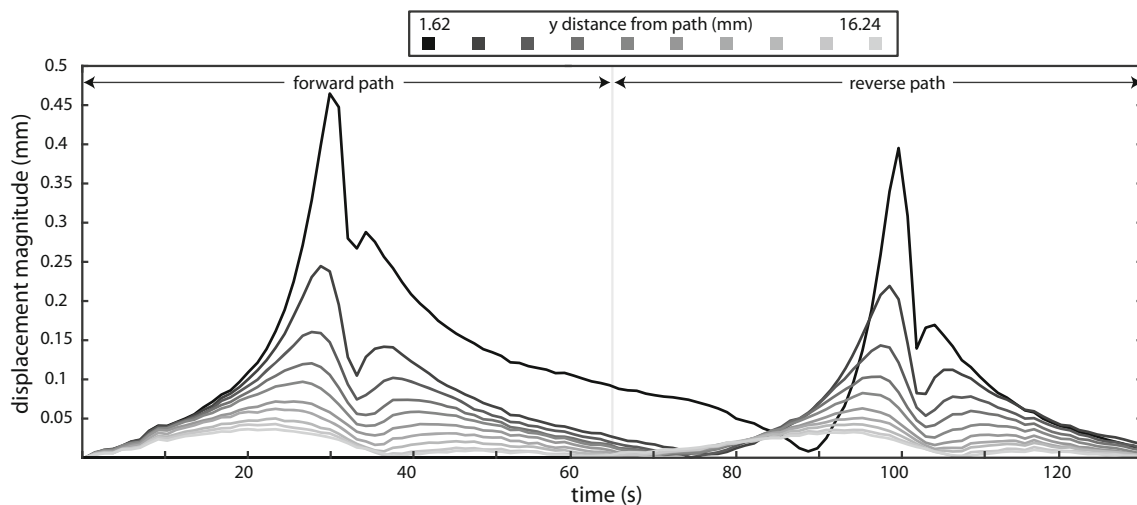


Fig. 11 The magnitude of displacement at the center of the needles path in the x-direction and at various distances from the needles path in the y direction as a function of time. The needle travels its full distance at 60 s then reverses direction to retrace its path

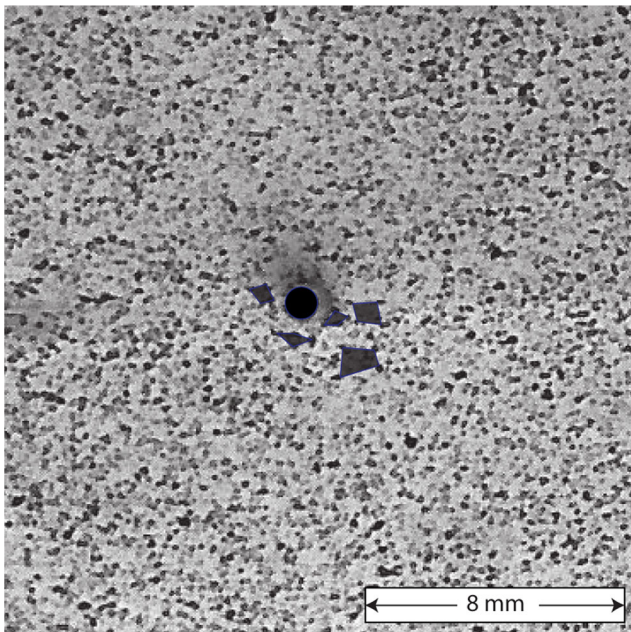


Fig. 12 A zoomed in image of the speckle pattern. Because of the white paint layer, the syringe and upper portion of the needle cannot be seen. Within the speckle pattern, five elements are identified by the corners of each speckle to form an element which will be distorted by the needle

Since the cross section of the cylinder and sphere are the same, it makes sense that the velocity fields, and possibly the displacement fields would be similar. Interactions between multiple needles may have the same characteristics as the work done by Othmane et al. [14] which measured the interaction between two spheres dropped at various distances from each other. The results of this work found that the minimum distance of separation to impart negligible effects upon each other is five diameters. Although the comparison of our result to the literature is not perfect, it is important to realize that subtle changes to the pH and concentration of Carbomer likely change the result substantially, so only the general trends should be compared. The DIC technique presented here allows for a broader range of analysis to be conducted and may be useful in furthering these areas of research.

The boundary between the fluid and solid region of yield stress materials have also been studied for circular cross sections in an infinite plane using numerical simulations [11, 14, 15, 20]. The results of these simulations show that the fluid region decreases with increasing Oldroyd numbers. Fig. 14 shows the same relationship since the Oldroyd number increases with decreasing velocity and increasing diameters.

The displacement of a region of the GSM was found and plotted for various distances away from the needle path in Fig. 11. This plot shows that the permanent deformation resulting from a forward pass can be reduced to almost zero net displacement by reversing the needle through the same path. Since we expect elastic deformation to return to net zero displacement when reversed, this analysis can allow us to

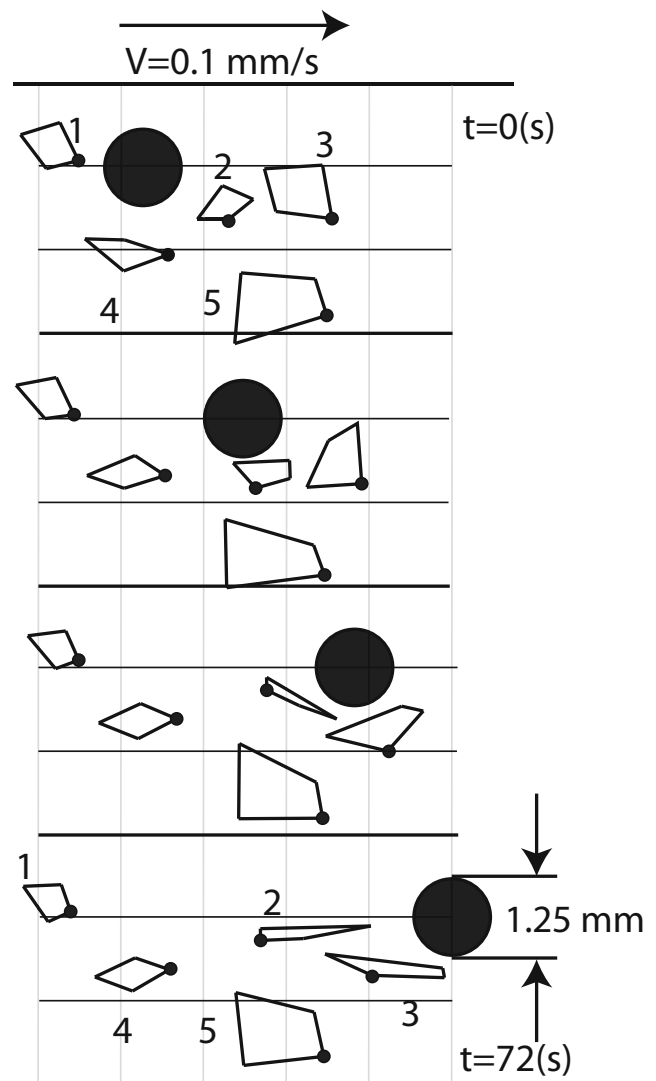


Fig. 13 The deformation of the GSM can be visualized using the five elements from Fig.12 at various locations surrounding the needle

differentiate between elastic and non-elastic regions. At two needle diameters away we can see that there is high permanent deformation of $100\ \mu\text{m}$ resulting from the forward pass and recovers to $20\ \mu\text{m}$ after the reverse pass.

Future Work

Although this method of determining the bulk in-plane deformation of a granular medium has been shown to produce high-quality results, there are still many improvements that can be made. For instance, since the out-of-plane distortion is not captured, we are unable to study the displacements at the needle tip since a large portion of that displacement is out of plane. The out-of-plane displacement can be measured however by slightly modifying the setup to include a stereo vision system and employing a 3D DIC analysis. Furthermore, a

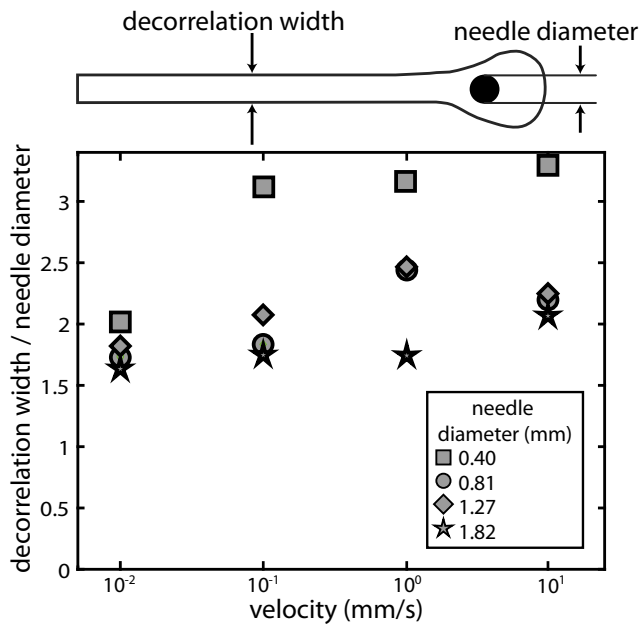


Fig. 14 The decorrelation width divided by the needle diameter is assumed to be closely related to the fluidized region. This region seems to stay relatively constant for each needle size with respect to the needle velocity

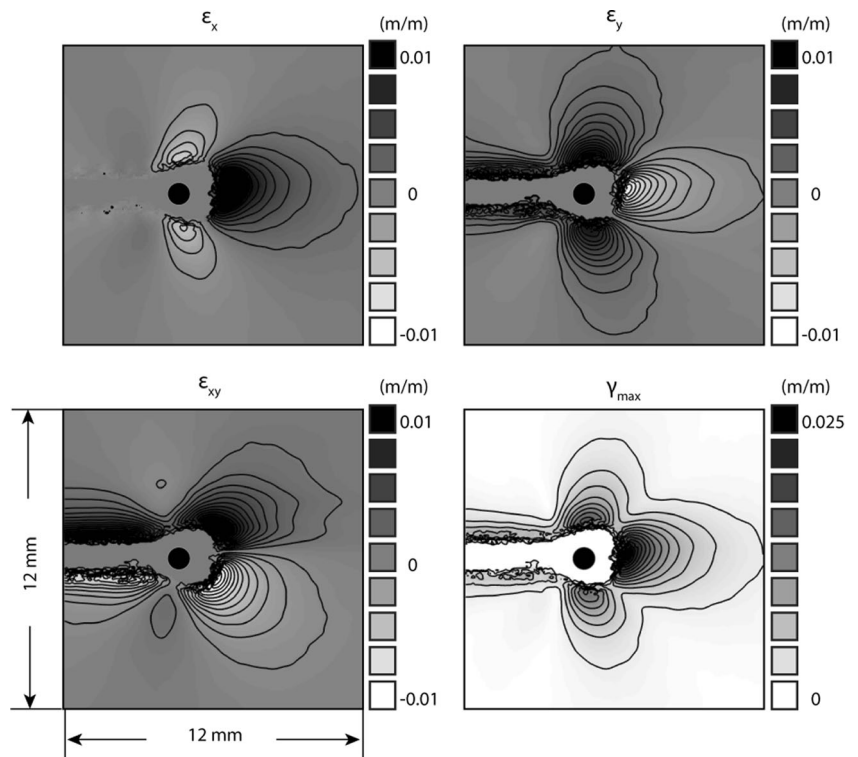
digital volumetric correlation (DVC) of the displacement can be found by varying the distance of the needle to the speckle pattern, measuring the 3D deformation of each plane and layering the results in a 3D matrix. This technique is similar

to existing experimental techniques on the bulk deformation of soft gels which utilize confocal microscopy to determine the plane and randomly scattered glass beads as the speckle pattern [28]. Another possible method for measuring volumetric displacement uses three speckle patterns at mutually orthogonal planes. As the needle moves through the volume, the displacements captured on each plane can be combined to show the x, y, and z components of displacement as a function of the distance of the plane from the needle.

The displacement and strain field around the tip of the needle during printing is likely to be very different from the results in this paper since the GSM is filled with material behind the needle and thus does not collapse. A thorough study of this displacement field will be conducted to better describe the displacements on the printing plane. The shape of the needle may also play an important role in determining the displacement and strain field within the volume, and various shapes including square, airfoil, and triangular needles will be tested. Since the interaction between the granular medium and the needle is a function of the strain rate, the various shapes will likely cause different flow conditions. These flow conditions will have an effect on how the transition region from solid to liquid states. Since the diameter of the needle did not have a large effect on the far-field behavior of the GSM, the far-field displacements may not change significantly in regards to the needle shape.

The evidence of memory in the GSM deformation is very interesting and has the potential to affect the printing process

Fig. 15 The strain analysis for the 0.81 mm diameter needle at 1 mm/s. The window is magnified to a 12 × 12 mm area around the needle tip



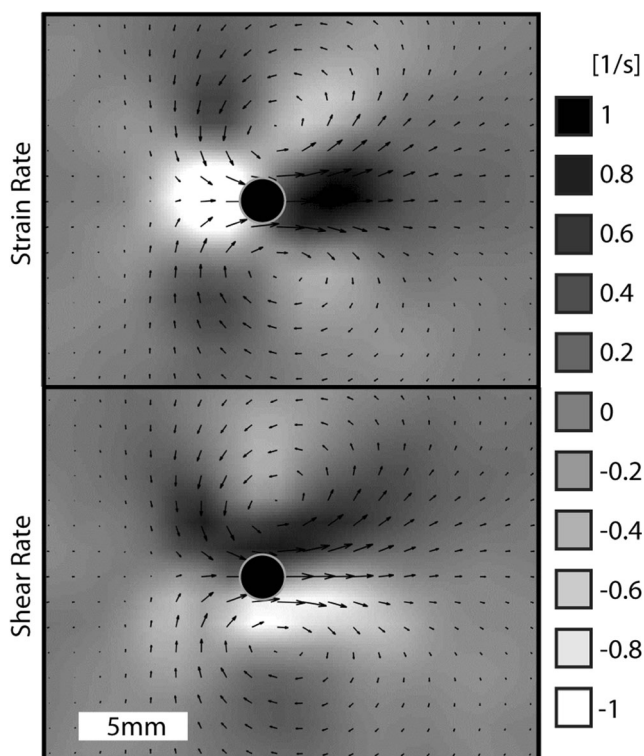


Fig. 16 The velocity field is superposed on top of the strain and shear rate field for the 0.81 mm needle at a velocity of 1 mm/s

in significant ways. A better understanding of this effect is vital to predicting total deformation of the volume while printing. By dragging a needle through the medium at parallel paths separated by a variable distance, the separation distance needed to nullify this memory effect can be found. This effect may also be time dependent, so a test will be conducted which keeps the path separation constant, but varies the rest time between experiments. Furthermore, the macrostructure of the Carbomer before and after the needle is dragged through an area should be imaged so we may gain intuition for the physical process taking place.

The interaction between multiple needles moving through the medium is of great interest and will need to be studied in great detail. Using two needles moving in parallel or perpendicular directions, the corresponding displacement fields will be analyzed to determine the distance each needle must be from one another to minimize the effect each has on one another.

Conclusion

We have presented a method to measure the bulk deformations within a yield stress fluid using DIC and PIV analysis. The ability to print a speckle pattern with random features into a container filled with the GSM allows for the measurement of large deformations. The displacements due to a cylindrical needle of various diameter and moving at various speeds were

found. The magnitudes of displacement were determined as a function of distance from the needle path and time history. Results show that near the needle there is a region of yielded/fluidized material and away from the needle path the material acts as a viscoelastic solid. Permanent deformation decreases with increased distance from the path and recovery is enhanced by reversing back through the path.

References

- Bhattacharjee T, Zehnder SM, Rowe KG et al (2015) Writing in the granular gel medium. *Sci Adv* 1:e1500655–e1500655. <https://doi.org/10.1126/sciadv.1500655>
- Curran SJ, Hayes RE, Afacan A et al (2002) Properties of Carbopol solutions as models for yield-stress fluids. *J Food Sci* 67:176–180. <https://doi.org/10.1111/j.1365-2621.2002.tb11379.x>
- Kim JY, Song JY, Lee EJ, Park SK (2003) Rheological properties and microstructures of Carbopol gel network system. *Colloid Polym Sci* 281:614–623. <https://doi.org/10.1007/s00396-002-0808-7>
- Boland T, Xu T, Damon B, Cui X (2006) Application of inkjet printing to tissue engineering. *Biotechnol J* 1:910–917. <https://doi.org/10.1002/biot.200600081>
- Leblanc KJ, Niemi SR, Bennett AI et al (2016) Stability of high speed 3D printing in liquid-like solids. *ACS Biomater Sci Eng* 2:1796–1799. <https://doi.org/10.1021/acsbomaterials.6b00184>
- Miller JS (2014) The billion cell construct: will three-dimensional printing get us there? *PLoS Biol* 12:1–9. <https://doi.org/10.1371/journal.pbio.1001882>
- Muth JT, Vogt DM, Truby RL et al (2014) Embedded 3D printing of strain sensors within highly stretchable elastomers. *Adv Mater* 26:6307–6312. <https://doi.org/10.1002/adma.201400334>
- Nishiyama Y, Nakamura M, Henmi C et al (2009) Development of a three-dimensional bioprinter: construction of cell supporting structures using hydrogel and state-of-the-art inkjet technology. *J Biomech Eng* 131:35001. <https://doi.org/10.1115/1.3002759>
- Wu W, Deconinck A, Lewis JA (2011) Omnidirectional printing of 3D microvascular networks. *Adv Mater* 23:178–183. <https://doi.org/10.1002/adma.201004625>
- Atapattu DD, Chhabra RP, Uhlherr PHT (1995) Creeping sphere motion in Herschel-Bulkley fluids: flow field and drag. *J Nonnewton Fluid Mech* 59:245–265. [https://doi.org/10.1016/0377-0257\(95\)01373-4](https://doi.org/10.1016/0377-0257(95)01373-4)
- Deglo De Besses B, Magnin A, Jay P (2003) Viscoplastic flow around a cylinder in an infinite medium. *J Nonnewton Fluid Mech* 115:27–49. [https://doi.org/10.1016/S0377-0257\(03\)00169-1](https://doi.org/10.1016/S0377-0257(03)00169-1)
- Holenberg Y, Lavrenteva OM, Liberzon A et al (2013) PTV and PIV study of the motion of viscous drops in yield stress material. *J Nonnewton Fluid Mech* 193:129–143. <https://doi.org/10.1016/j.jnnfm.2012.09.013>
- Holenberg Y, Lavrenteva OM, Shavit U, Nir A (2012) Particle tracking velocimetry and particle image velocimetry study of the slow motion of rough and smooth solid spheres in a yield-stress fluid. *Phys Rev E - Stat Nonlinear, Soft Matter Phys* 86:1–6. <https://doi.org/10.1103/PhysRevE.86.066301>
- Merkak O, Jossic L, Magnin A (2006) Spheres and interactions between spheres moving at very low velocities in a yield stress fluid. *J Nonnewton Fluid Mech* 133:99–108. <https://doi.org/10.1016/j.jnnfm.2005.10.012>

15. Mossaz S, Jay P, Magnin A (2012) Non-recirculating and recirculating inertial flows of a viscoplastic fluid around a cylinder. *J Nonnewton Fluid Mech* 177–178:64–75. <https://doi.org/10.1016/j.jnnfm.2012.04.008>
16. Mossaz S, Jay P, Magnin A (2012) Experimental study of stationary inertial flows of a yield-stress fluid around a cylinder. *J Nonnewton Fluid Mech* 189–190:40–52. <https://doi.org/10.1016/j.jnnfm.2012.10.001>
17. Putz AMV, Burghilea TI, Frigaard IA, Martinez DM (2008) Settling of an isolated spherical particle in a yield stress shear thinning fluid. *Phys Fluids*. <https://doi.org/10.1063/1.2883937>
18. Tokpavi DL, Jay P, Magnin A, Jossic L (2009) Experimental study of the very slow flow of a yield stress fluid around a circular cylinder. *J Nonnewton Fluid Mech* 164:35–44. <https://doi.org/10.1016/j.jnnfm.2009.08.002>
19. Zisis T, Mitsoulis E (2002) Viscoplastic flow around a cylinder kept between parallel plates. *J Nonnewton Fluid Mech* 105:1–20. [https://doi.org/10.1016/S0377-0257\(02\)00025-3](https://doi.org/10.1016/S0377-0257(02)00025-3)
20. Tokpavi DL, Magnin A, Jay P (2008) Very slow flow of Bingham viscoplastic fluid around a circular cylinder. *J Nonnewton Fluid Mech* 154:65–76. <https://doi.org/10.1016/j.jnnfm.2008.02.006>
21. Keane RD, Adrian RJ (1992) Theory of cross-correlation analysis of PIV images. *Appl Sci Res* 49:191–215. <https://doi.org/10.1007/BF00384623>
22. Nogueira J, Lecuona A, Rodríguez PA et al (2005) Limits on the resolution of correlation PIV iterative methods. Practical implementation and design of weighting functions. *Exp Fluids* 39:314–321. <https://doi.org/10.1007/s00348-005-1017-1>
23. Crammond G, Boyd SW, Dulieu-Barton JM (2013) Speckle pattern quality assessment for digital image correlation. *Opt Lasers Eng* 51: 1368–1378. <https://doi.org/10.1016/j.optlaseng.2013.03.014>
24. Mitsoulis E (2004) On creeping drag flow of a viscoplastic fluid past a circular cylinder: wall effects. *Chem Eng Sci* 59:789–800. <https://doi.org/10.1016/j.ces.2003.09.041>
25. Benmouffok-Benbelkacem G, Caton F, Baravian C, Skali-Lami S (2010) Non-linear viscoelasticity and temporal behavior of typical yield stress fluids: Carbopol, xanthan and ketchup. *Rheol Acta* 49: 305–314. <https://doi.org/10.1007/s00397-010-0430-4>
26. Blaber J, Adair B, Antoniou A (2015) Ncorr: open-source 2D digital image correlation Matlab software. *Exp Mech* 55:1105–1122. <https://doi.org/10.1007/s11340-015-0009-1>
27. Thielicke W, Stamhuis EJ (2014) PIVlab – Towards User-friendly, Affordable and Accurate Digital Particle Image Velocimetry in MATLAB. *Journal of Open Research Software*. <http://dx.doi.org/10.5334/jors.bl>
28. Jop P, Mansard V, Chaudhuri P et al (2012) Microscale rheology of a soft glassy material close to yielding. *Phys Rev Lett* 108:1–5. <https://doi.org/10.1103/PhysRevLett.108.148301>